

Rapid transformation of ambient absorbing aerosols from West African biomass burning

Huihui Wu¹, Jonathan W Taylor¹, Justin M Langridge², Chenjie Yu¹, James D Allan^{1,3}, Kate Szpek², Michael I Cotterell^{4,*}, Paul I Williams^{1,3}, Michael Flynn¹, Patrick Barker¹, Cathryn Fox², Grant Allen¹,
5 James Lee^{5,6}, and Hugh Coe¹

¹Department of Earth and Environmental Sciences, University of Manchester, Manchester, UK

²Met Office, Fitzroy Road, Exeter, EX1 3PB, UK

³National Centre for Atmospheric Science, University of Manchester, Manchester, UK

⁴College of Engineering, Mathematics and Physical Sciences, University of Exeter, Exeter, UK.

10 ⁵Wolfson Atmospheric Chemistry Laboratories, Department of Chemistry, University of York, York YO10 5DD, UK

⁶National Centre for Atmospheric Sciences, University of York, York YO10 5DD, UK

*Now at School of Chemistry, University of Bristol, Bristol, United Kingdom

Correspondence to: Hugh Coe (hugh.coe@manchester.ac.uk)

Supplementary

15 S1 Calculation methods

S1.1 Fire combustion and emission information

The modified combustion efficiency (MCE) is defined as the excess mixing ratio of carbon dioxide (CO₂) over the background to the sum of the excess mixing ratios of carbon monoxide (CO) and CO₂: $MCE = \Delta CO_2 / (\Delta CO + \Delta CO_2)$ (Yokelson et al., 2009). For an identified smoke plume, MCE can be also calculated by determining the slope between CO and CO₂ using an unconstrained linear orthogonal distance regression (ODR) and subsequently solved for $MCE = 1 / (1 + \delta CO / \delta CO_2)$. Emission information can be represented in two basic forms: enhancement ratio (ER) and emission factor (EF). The ER of a species (X) can be calculated by dividing the excess X by the excess concentration of a reference species Y ($\Delta X / \Delta Y$), which can be also calculated by determining the slope between X and Y using from unconstrained linear ODR fitting (Yokelson et al., 2013). The reference species chosen for this work was CO, as it is relatively inert in the timescale of
25 these measurements and had a relatively stable regional background concentration during the campaign. The EF of X is defined as the mass of X emitted (in grams) with per kilogram of dry matter burnt (Andreae and Merlet, 2001). Using the ER calculated for each species, the EF of X is given by equation (S1) as below:

$$EF_X = F_C \cdot 1000 (\text{g kg}^{-1}) \cdot \frac{M_X}{M_C} \cdot \frac{C_X}{C_{total}} \quad (\text{S1})$$

where F_C is the fraction of carbon in the fuel source. In this study, a value of 0.475 is used for F_C to represent African
30 biomass burning (Andreae and Merlet, 2001). M_X and M_C are the molecular weights of species X and carbon respectively.

The term C_X / C_{total} is the molar ratio of species X to total carbon in the plume, which is calculated using equation (S2):

$$\frac{C_X}{C_{total}} = \frac{ER_X \frac{X}{CO}}{1 + \frac{\Delta CO_2}{\Delta CO} + \frac{\Delta CH_4}{\Delta CO}} \quad (S2)$$

In Eq. (S2), total carbon in the fire plume was assumed to be the sum of CO, CO₂ and CH₄ emitted. However, as all carbon containing species could not be measured in this study, the total carbon present in the plume may be underestimated by 1-2% (Yokelson et al. 1999).

The calculation methods of MCE and emission information follows the work by Barker et al., (2020). For freshly emitted plumes (< 0.5 h), the background concentrations were determined immediately before entry into and after exiting out of the plume. The same background periods were chosen for all species in each fresh plume, to ensure that calculations were comparable and not influenced by inconsistent background criteria. The area under the plume was determined by integrating the peak in the concentration versus time data series (Fig. S2a) and the background areas were removed, which gave the ΔCO , ΔCO_2 , ΔX and ΔCH_4 . These values were then used to determine the MCE and ER and EF of X in each fresh plume. When calculating the ER of OA to CO, the 1-Hz CO data were averaged into the AMS time base. The analysis uncertainty includes the 1-sigma standard deviation and the instruments uncertainty. For transported smoke over continent and ocean (~1 h; ~3–6 h; ~9–12 h), an unconstrained linear ODR fitting between all in-plume points of CO₂ and in-plume points of CO is used to determine MCE. The fitting between all in-plume points of X and in-plume points of CO is used to determine the ER and EF. When calculating the ER of OA to CO in transported smoke, the 1-Hz CO data were also averaged into the AMS time base. The analysis uncertainty includes the fit error and the instruments uncertainty.

S1.2 Absorption attribution using the AAE methods

BrC absorption at a short wavelength λ_1 ($B_{Abs-BrC, \lambda_1}$) can be derived by subtracting BC absorption (B_{Abs-BC, λ_1}) from the total aerosol absorption (Lack and Langridge, 2013) via

$$B_{Abs-BrC, \lambda_1} = B_{Abs, \lambda_1} - B_{Abs-BC, \lambda_1}$$

where absorption B_{Abs, λ_1} is the measured absorption at the short wavelength λ_1 . BC absorption at λ_1 (B_{Abs-BC, λ_1}) can be obtained using the AAE value of BC (AAE_{BC}) via

$$B_{Abs-BC, \lambda_1} = B_{Abs-\lambda_2} \times (\lambda_2/\lambda_1)^{AAE_{BC}}$$

where B_{Abs, λ_2} is the total aerosol absorption measured at a longer wavelength λ_2 (658 nm), which is assumed to have no contributions from BrC or dust (Lack and Langridge, 2013). The uncertainty involved in attributing BrC and BC absorption at short wavelengths has been explored explicitly by Lack and Langridge (2013). This uncertainty is primarily from the uncertainty in the assumed AAE_{BC} . The AAE_{BC} used in this study includes the AAEs ($AAE_{405-658}$ and $AAE_{514-658}$) from optical modelling. More details about the AAEs from optical modelling are described in the main text, Sect. 2.3 and 3.4.

60 **S1.3 Estimation of organic-linked nitrate**

In AMS measurements, the nitrate is detected at m/z 30 and m/z 46, representing the ions of NO^+ and NO_2^+ respectively. Inorganic (i.e. ammonium nitrate, NH_4NO_3 and mineral nitrate) and organic nitrates both contribute to the two peaks. Mineral nitrate salts, i.e. NaNO_3 and KNO_3 , are unlikely to be measured by the AMS in this study, due to their low vaporization efficiency and large size. Here, we determined the fractional contribution of NH_4NO_3 and organic-linked nitrate to the total observed signals at these two peaks, following the methods proposed by Farmer et al. (2010) and modified by Kiendler-Scharr et al. (2016). The fraction of organic-linked nitrate in the measured nitrate ($X_{\text{Org-NO}_3}$) is estimated using the equation (S3):

$$X_{\text{Org-NO}_3} = \frac{(1 + R_{\text{ON}}) \times (R_{\text{measured}} - R_{\text{calib}})}{(1 + R_{\text{measured}}) \times (R_{\text{ON}} - R_{\text{calib}})} \quad (\text{S3})$$

The R_{measured} is the measured intensity ratio of m/z 46 and m/z 30. R_{calib} is the ratios measured during NH_4NO_3 calibrations. R_{ON} is the m/z 46 over 30 ratios from organic nitrogen. R_{ON} is set to 0.1 following considerations presented by Kiendler-Scharr et al. (2016), which is the minimum $\text{NO}_2^+/\text{NO}^+$ ratio observed in field datasets and gives the lower limits of $X_{\text{Org-NO}_3}$. The R_{ON} value of 0.1 has been used in many previous studies (e.g. Tiitta et al., 2016; Reyes-Villegas et al., 2018). The mass concentration of organic-linked nitrate is then calculated by multiplying the total nitrate measured by the AMS with $X_{\text{Org-NO}_3}$. The method proposed by Farmer et al. (2010) is based on the high-resolution-ToF AMS (HR-ToF AMS) measurements, where R_{measured} is the measured $\text{NO}_2^+/\text{NO}^+$ ratio rather than the ratio of m/z 46 and m/z 30 used in this study. With the C-ToF AMS used in this study, the interference of some ions from organics (i.e. CH_2O^+ , CH_4N^+ and C_2H_6^+ at $m/z = 30$ and CH_2O_2^+ and $\text{C}_2\text{H}_6\text{O}^+$ at $m/z = 46$) cannot be separated at these two peaks, which would add uncertainties in the ambient ratios for nitrate. However, previous laboratory and ambient BB studies using HR-ToF AMS indicate that the interference of these ions may be small (e.g. Reyes-Villegas et al., 2018). In this study, the ratios of organic-linked nitrate over total OA mass are investigated with ageing process.

S2 Optical modelling

S2.1 Determination of the size and mixing state of BC-containing particles

In this study, we simulated the MAC and AAE of coated BC with non-absorbing coatings, using a variety of optical models. Firstly, we determined the size and mixing state of BC-containing particles from the single-particle measurements of BC mass and scattering cross-section from the SP2. This process is based on previous works of Taylor et al. (2015, 2020) and Liu et al., (2017). Taylor et al. (2015) described the steps to calculate physical parameters of BC-containing particles, with the SP2 measurements and a scattering model using core/shell Mie theory. The main steps based on Taylor et al. (2015) include: 1) A 2-D lookup Mie table was produced containing scattering cross-sections at $\lambda = 1064$ nm, for core diameter of $80 \leq D_c \leq 600$ nm and coated diameter of $80 \leq D_p \leq 1500$ nm, with 1 nm resolution. 2) The single-particle BC core mass (M_{BC}) was converted to the spherical-equivalent D_c , using a BC density of 1.8 g cm^{-3} . 3) Then, the single-particle data of D_c

and scattering cross-section was processed to calculate the single-particle spherical-equivalent D_P through the generated Mie table. In this study, an empirical correction from Liu et al. (2017) was also implemented into these processes from Taylor et al. (2015). Liu et al. (2017) introduced the mass ratio of non-BC to BC (MR), to the core/shell Mie simulations and compared with laboratory and field measurements. Liu et al. (2017) found that, for $MR > 3$, the measured scattering cross-section at 1064 nm is best reproduced by the core/shell Mie model, for $MR < 3$, particles do not scatter light exactly at 1064 nm as described by the model. An empirical correction to the core/shell Mie model was then designed for particles with $MR < 3$, to fit the measurements. Thus, we corrected the 2-D lookup Mie table using this empirical correction, by calculating the equivalent MR with the diameters and assumed densities of the core and coating. The single-particle spherical-equivalent D_P was also re-calculated through the corrected Mie table. We converted the single-particle D_P/D_C ratio derived from above processes to MR and generated a 2-D distribution of MR vs. M_{BC} . For SP2 measurements, not all detected particles have a successful LEO fitting to measure the scattering cross-section of BC-containing particles at 1064 nm, as most particles in the small size range do not scatter enough light to be detected and the detected signal of particles at large sizes is noisy due to limited number concentration (Liu, D. et al., 2014; Taylor et al., 2015). Due to this limited efficiency in the detection range for the scattering channel, the MR vs. M_{BC} distribution was corrected for the size-dependent detection efficiency of the SP2 instrument, following the methods described by Taylor et al. (2015, 2020).

S2.2 Optical models and parametrisations

Core/shell Mie model

For BC-containing particles, we assumed a concentric sphere core/shell configuration, and used Mie theory to calculate the absorption cross-sections. Here, we used the Scattlnlay Mie code (Pena and Pal, 2009), these algorithms were compiled as an external operation (XOP) for Igor Pro (Wavemetrics). Using this package, we generated a 2-D table of absorption cross-section following core/shell Mie theory, which is corresponding to the same grid of the 2-D distribution of MR vs. M_{BC} from measurement data. We used a full 2-D bin scheme as bulk absorption calculations. The MAC of coated BC was calculated by dividing the integrated bulk absorption cross-section of coated BC by the BC mass. These calculations were termed “CS”.

In Mie models, the intensity of light decreases when penetrating through an absorbing sphere, shielding the centre. Thus, for large particles, the centre of a spherical particle is effectively shielded from exposure to light. In reality, BC is a non-spherical fractal aggregate with a porous structure and a high surface-to-volume ratio. This high surface area relative to the total BC mass allows light to fully interact with the BC component and the shielding effect is diminished (e.g. Chakrabarty and Heinson, 2018). Therefore, the shielding effect in Mie models leads to an underestimation of light absorption for the BC particles. Taylor et al. (2020) has discussed the underprediction of MAC at short wavelengths from the core/shell Mie model. To explicitly demonstrate the effect of this skin-depth shielding, we also used another implementation in the core-shell Mie model, termed “CS- E_{Abs} ”, where the core/shell Mie model is used to calculate E_{Abs} . The modelled E_{Abs} is determined as the ratio of the simulated bulk absorption cross-section for coated BC to that for uncoated BC from the “CS” method. The MAC

of coated BC was then calculated by multiplying the modelled E_{Abs} and the MAC of uncoated BC (MAC_{BC}) from Bond and Bergstrom (2006). This CS- E_{Abs} method corrects the MAC for clear-coated BC using MAC_{BC} values ($7.5 \text{ m}^2 \text{ g}^{-1}$ at $\lambda = 550$ nm, with $\text{AAE} = 1$) that are summarised from previous literatures and are commonly accepted as best estimates. In addition, we considered different refractive index of BC (m_{BC}) assumed in the core/shell Mie model, as listed in table S1.

Table S1. The different values of m_{BC} used in this study.

m_{BC}	reference
1.75 – 0.63i	Bond and Bergstrom ,2006
1.80 – 0.67i	Bond and Bergstrom ,2006
1.85 – 0.71i	Bond and Bergstrom ,2006
1.90 – 0.75i	Bond and Bergstrom ,2006
1.95 – 0.79i	Bond and Bergstrom ,2006
2.26 – 1.26i	Moteki et al., 2010

Parameterisations

1) Liu- E_{Abs}

Liu et al. (2017) introduced an empirical correction to the core/shell Mie models based on laboratory and atmospheric observations. They conducted ambient measurements of aerosols from different combustion sources, and a laboratory chamber study of fresh and aged diesel soot. The mixing state of BC particles was quantified using morphology-independent factor of mass ratio, MR, which was measured by a novel coupling of a Centrifugal Particle Mass Analyser (CPMA, Cambustion) and a single-particle soot photometer (SP2). The CPMA can select particles of known and quantifiable mass. The SP2 can provide the measurements of single-particle BC mass and scattering cross-section of BC-particles at 1064 nm. The wavelength-dependent absorption coefficient was measured by a photoacoustic soot spectrometer (PASS, Droplet Measurement Technologies, Boulder, Co). A thermal denuder heated the sample to 400°C in order to remove non-BC material. The measured E_{Abs} and scattering enhancement (E_{Sca}) were determined by comparing these thermally-denuded measurements to measurements of the unheated sample. Liu et al. (2017) compared the SP2-measured E_{Sca} of BC at 1064 nm to the simulated E_{Sca} at 1064 nm using different optical models. They found that, for particles with $\text{MR} < 1.5$, the measured E_{Sca} shows agreement with the optical model assuming externally mixed BC and non-BC components, i.e. E_{Sca} of 0. For particles with $\text{MR} > 3$, the measured scattering cross-section and E_{Sca} are best reproduced by the core/shell Mie model (“CS”). There also exists a transition zone for particles with MR between these two regimes. It is assumed that E_{Abs} behaves in a similar manner to E_{Sca} . Based on the comparison between “CS”-modelled and measured E_{Sca} at 1064 nm, Liu et al. (2017) corrected the “CS” by deriving an empirical fit to E_{Abs} and E_{Sca} , which uses an internally mixed fraction parameter (F_{in}). The corrections are expressed as:

$$E_{\text{Abs}} = E_{\text{Abs,CS}} \times F_{\text{in}} + (1 - F_{\text{in}}) \times 1$$

$$E_{\text{Sca}} = E_{\text{Sca,CS}} \times F_{\text{in}} + (1 - F_{\text{in}}) \times 1$$

where $F_{in} = 0$ (when $MR < 1.5$); $F_{in} = 0.57 \times MR - 0.74$ (when $1.5 < MR < 3$); $F_{in} = 1$ (when $MR > 3$).

150 The modelled bulk E_{abs} values using this approach are shown to be in good agreement with the measured E_{abs} in Liu et al. (2017). In this work, the m_{BC} for calculating core/shell Mie model is $1.85-0.71i$, as used by Liu et al. (2017). To calculate the coated MAC from “Liu- E_{Abs} ”, we multiplied the modelled “Liu- E_{Abs} ” by the MAC of uncoated BC from Bond and Bergstrom (2006).

2) Wu- E_{Abs}

155 Wu et al. (2018) introduced an empirical correction to core/shell Mie models based on model results which were constrained by BC micromorphology. In their study, different mixing states of BC-containing particles were constructed and modelled by a novel aggregate model, including the states of bare, partly coated, partially encapsulated, and heavily coated. These morphologies of BC-containing particles were based on the scanning electron microscope images. For bare BC, they were generated by the diffusion limited aggregation method, the aggregations of BC monomers were constructed with the
160 given fractal parameters. Non-BC material was then added to the surface of these aggregates for their partly coated states. To generate partially encapsulated BC, part of the aggregation was all inside the non-BC material, while the remaining outer aggregation was all outside the non-BC material. Further ageing gave heavily coated BC with BC monomers inside a non-BC particle. Wu et al. (2018) also used the MR measured from the CPMA and SP2, the ranges of MR were assumed for different mixing states of BC-containing particles. Optical properties of these constructed BC-containing particles were
165 calculated using the superposition T-matrix method and were averaged for different orientations of the particles. The simulated MAC values from the aggregate model showed good agreement with the measured MAC derived from the PASS and SP2. By comparing the core/shell Mie model and Aggregate model results, a correction coefficient is suggested to improve the core/shell Mie model predictions of E_{abs} by applying an exponential fitting function:

$$E_{Abs} = 0.92 + 0.11e^{(E_{Abs}-1.07) / 0.55}.$$

170 In this calculation, we calculated bulk absorption cross-section of coated BC using the core/shell Mie theory and the wavelength-dependent m_{BC} from Chang and Charalampopoulos (1990), as well as the bulk absorption cross-section if the coating thicknesses were zero. The ratio of coated BC absorption to uncoated BC absorption (as described under “CS- E_{Abs} ”) was corrected using the equation above to derive “Wu- E_{Abs} ”. To calculate the coated MAC from “Wu- E_{Abs} ”, we multiplied the modelled “Wu- E_{Abs} ” by the MAC of uncoated BC from Bond and Bergstrom (2006).

175 3) Chak- E_{Abs} and Chak-MAC

Chakrabarty and Heinson (2018) integrated modelled results and observational findings to establish scaling relationships for E_{Abs} and MAC_{BC} as a function of coating and BC mass. They generated BC aggregates using a fractal aerosol model and considered three morphologies of BC-containing particles, including bare, partly coated and partially encapsulated. The parameter of (M_{total} / M_{BC}) was defined as the ratio of total particle mass to the BC mass. The ranges of
180 (M_{total} / M_{BC}) were assumed for different mixing states of BC-containing particles. Chakrabarty and Heinson (2018) generated internally mixed BC aggregates with different (M_{total} / M_{BC}) and applied dipole-dipole approximation

electromagnetic theory to compute the orientationally averaged MAC_{BC} and E_{Abs} . They produced parameterisations representing the power-law scaling relations between the modelled E_{Abs} or MAC_{BC} with (M_{total} / M_{BC}) , which are expressed as:

$$185 \quad MAC = \left(\frac{3.6}{\lambda}\right) \left(\frac{M_{total}}{M_{BC}}\right)^{\frac{1}{3}}$$
$$E_{Abs} = \left(\frac{M_{total}}{M_{BC}}\right)^{\frac{1}{3}}$$

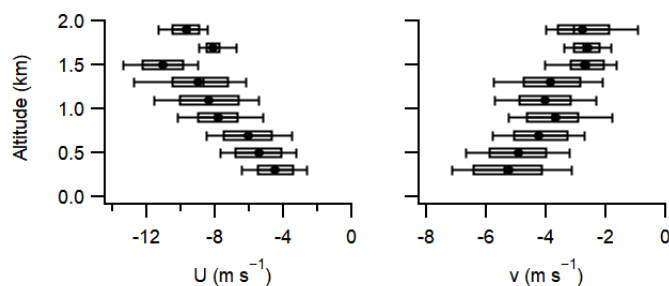
In this calculation, we generated 2-D tables of MAC and E_{Abs} using these equations, corresponding to the same grid of the 2-D distribution of MR vs. M_{BC} generated from measurement data. A 2-D bin scheme was used for bulk calculations of absorption cross-section and “Chak- E_{Abs} ”. The MAC of coated BC was calculated by dividing the integrated bulk absorption cross-section of coated BC by the integrated BC mass, termed “Chak- MAC ”. We also multiplied the modelled “Chak- E_{Abs} ” by the MAC of uncoated BC from Bond and Bergstrom (2006) to calculate the MAC of coated BC .

References

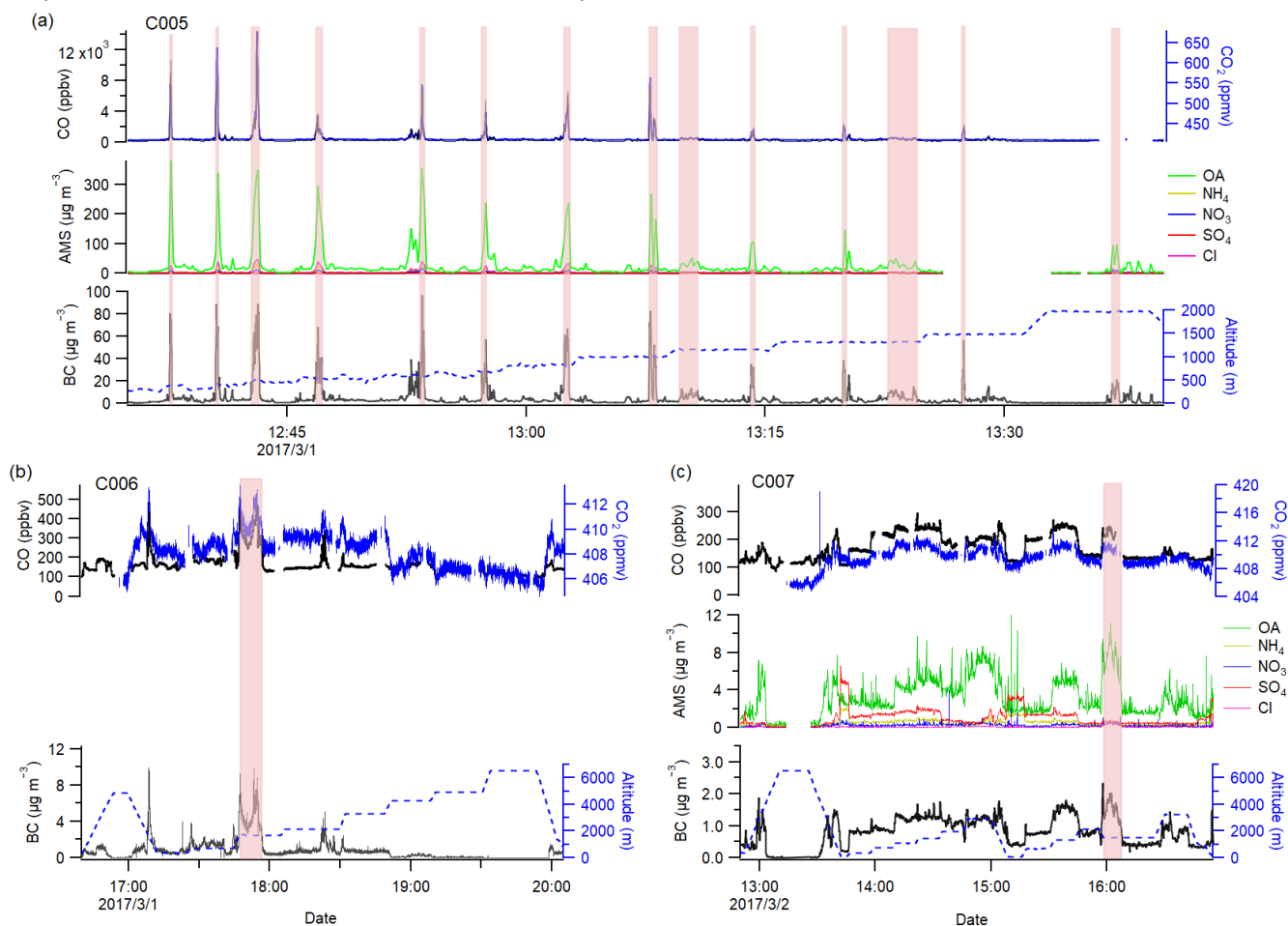
- Andreae, M. O. and Merlet, P.: Emission of trace gases and aerosols from biomass burning, *Global Biogeochem. Cy.*, 15, 955-966, <https://doi.org/10.1029/2000gb001382>, 2001.
- 195 Barker, P. A., Allen, G., Gallagher, M., Pitt, J. R., Fisher, R. E., Bannan, T., Nisbet, E. G., Bauguitte, S. J.-B., Pasternak, D., Cliff, S., Schimpf, M. B., Mehra, A., Bower, K. N., Lee, J. D., Coe, H., and Percival, C. J.: Airborne measurements of fire emission factors for African biomass burning sampled during the MOYA campaign, *Atmos. Chem. Phys.*, 20, 15443–15459, <https://doi.org/10.5194/acp-20-15443-2020>, 2020.
- Bond, T. C. and Bergstrom, R. W.: Light absorption by carbonaceous particles: An investigative review, *Aerosol Sci. Tech.*, 200 40, 27–67, <https://doi.org/10.1080/02786820500421521>, 2006.
- Chakrabarty, R. K. and Heinson, W. R.: Scaling laws for light absorption enhancement due to nonrefractory coating of atmospheric black carbon aerosol, *Phys. Rev. Lett.*, 121, 218701, <https://doi.org/10.1103/PhysRevLett.121.218701>, 2018.
- Chang, H.; Charalampopoulos, T. T. Determination of the wavelength dependence of refractive indices of flame soot. *Proc. R. Soc. Lond. A Math. Phys. Sci.*, 430, 577-591, <https://doi.org/10.1098/rspa.1990.0107>, 1990.
- 205 Farmer, D. K., Matsunaga, A., Docherty, K. S., Surratt, J. D., Seinfeld, J. H., Ziemann, P. J., and Jimenez, J. L.: Response of an aerosol mass spectrometer to organonitrates and organosulfates and implications for atmospheric chemistry, *P. Natl. Acad. Sci. USA*, 107, 6670–6675, <https://doi.org/10.1073/pnas.0912340107>, 2010.
- Kiendler-Scharr, A., Mensah, A. A., Friese, E., Topping, D., Nemitz, E., Prevot, A. S. H., Äijälä, M., Allan, J., Canonaco, F., Canagaratna, M., Carbone, S., Crippa, M., Dall'Osto, M., Day, D. A., De Carlo, P., Di Marco, C. F., Elbern, H., Eriksson, 210 A., Freney, E., Hao, L., Herrmann, H., Hildebrandt, L., Hillamo, R., Jimenez, J. L., Laaksonen, A., McFiggans, G., Mohr, C., O'Dowd, C., Otjes, R., Ovadnevaite, J., Pandis, S. N., Poulain, L., Schlag, P., Sellegri, K., Swietlicki, E., Tiitta, P.,

- Vermeulen, A., Wahner, A., Worsnop, D., and Wu, H. C.: Ubiquity of organic nitrates from nighttime chemistry in the european submicron aerosol, *Geophys. Res. Lett.*, 43, 7735–7744, <https://doi.org/10.1002/2016gl069239>, 2016.
- 215 Lack, D. A. and Langridge, J. M.: On the attribution of black and brown carbon light absorption using the Ångström exponent, *Atmos. Chem. Phys.*, 13, 10535–10543, <https://doi.org/10.5194/acp-13-10535-2013>, 2013.
- Liu, D., Whitehead, J., Alfarra, M. R., Reyes-Villegas, E., Spracklen, D. V., Reddington, C. L., Kong, S., Williams, P. I., Ting, Y.-C., Haslett, S., Taylor, J. W., Flynn, M. J., Morgan, W. T., McFiggans, G., Coe, H., and Allan, J. D.: Black-carbon absorption enhancement in the atmosphere determined by particle mixing state, *Nat. Geosci.*, 10, 184–188, <https://doi.org/10.1038/ngeo2901>, 2017.
- 220 Moteki, N., Kondo, Y., and Nakamura, S.: Method to measure refractive indices of small nonspherical particles: application to black carbon particles, *J. Aerosol. Sci.*, 41, 513–521, <https://doi.org/10.1016/j.jaerosci.2010.02.013>, 2010.
- Taylor, J. W., Allan, J. D., Liu, D., Flynn, M., Weber, R., Zhang, X., Lefer, B. L., Grossberg, N., Flynn, J., and Coe, H.: Assessment of the sensitivity of core / shell parameters derived using the single-particle soot photometer to density and refractive index, *Atmos. Meas. Tech.*, 8, 1701–1718, <https://doi.org/10.5194/amt-8-1701-2015>, 2015.
- 225 Taylor, J. W., Wu, H., Szpek, K., Bower, K., Crawford, I., Flynn, M. J., Williams, P. I., Dorsey, J., Langridge, J. M., Cotterell, M. I., Fox, C., Davies, N. W., Haywood, J. M., and Coe, H.: Absorption closure in highly aged biomass burning smoke, *Atmos. Chem. Phys.*, 20, 11201–11221, <https://doi.org/10.5194/acp-20-11201-2020>, 2020.
- Tiitta, P., Leskinen, A., Hao, L., Yli-Pirilä, P., Kortelainen, M., Grigonyte, J., Tissari, J., Lamberg, H., Hartikainen, A., Kuuspalo, K., Kortelainen, A.-M., Virtanen, A., Lehtinen, K. E. J., Komppula, M., Pieber, S., Prévôt, A. S. H., Onasch, T.
- 230 B., Worsnop, D. R., Czech, H., Zimmermann, R., Jokiniemi, J., and Sippula, O.: Transformation of logwood combustion emissions in a smog chamber: formation of secondary organic aerosol and changes in the primary organic aerosol upon daytime and nighttime aging, *Atmos. Chem. Phys.*, 16, 13251–13269, <https://doi.org/10.5194/acp-16-13251-2016>, 2016.
- Pena, O. and Pal, U.: Scattering of electromagnetic radiation by a multilayered sphere, *Comput. Phys. Commun.*, 180, 2348–2354, <https://doi.org/10.1016/j.cpc.2009.07.010>, 2009.
- 235 Reyes-Villegas, E., Priestley, M., Ting, Y.-C., Haslett, S., Bannan, T., Le Breton, M., Williams, P. I., Bacak, A., Flynn, M. J., Coe, H., Percival, C., and Allan, J. D.: Simultaneous aerosol mass spectrometry and chemical ionisation mass spectrometry measurements during a biomass burning event in the UK: insights into nitrate chemistry, *Atmos. Chem. Phys.*, 18, 4093–4111, <https://doi.org/10.5194/acp-18-4093-2018>, 2018.
- Wu, Y., Cheng, T., Liu, D., Allan, J. D., Zheng, L., and Chen, H.: Light Absorption Enhancement of Black Carbon Aerosol
- 240 Constrained by Particle Morphology, *Environ. Sci. Technol.*, 52, 6912–6919, <https://doi.org/10.1021/acs.est.8b00636>, 2018.
- Yokelson, R. J., Goode, J. G., Ward, D. E., Susott, R. A., Babbitt, R. E., Wade, D. D., Bertschi, I., Griffith, D. W. T., and Hao, W. M.: Emissions of formaldehyde, acetic acid, methanol, and other trace gases from biomass fires in North Carolina measured by airborne Fourier transform infrared spectroscopy, *J. Geophys. Res.*, 104(D23), 30109–30126, <https://doi.org/10.1029/1999JD900817>, 1999.

- 245 Yokelson, R. J., Crounse, J. D., DeCarlo, P. F., Karl, T., Urbanski, S., Atlas, E., Campos, T., Shinozuka, Y., Kapustin, V., Clarke, A. D., Weinheimer, A., Knapp, D. J., Montzka, D. D., Holloway, J., Weibring, P., Flocke, F., Zheng, W., Toohey, D., Wennberg, P. O., Wiedinmyer, C., Mauldin, L., Fried, A., Richter, D., Walega, J., Jimenez, J. L., Adachi, K., Buseck, P. R., Hall, S. R., and Shetter, R.: Emissions from biomass burning in the Yucatan, *Atmos. Chem. Phys.*, 9, 5785–5812, <https://doi.org/10.5194/acp-9-5785-2009>, 2009.
- 250 Yokelson, R. J., Andreae, M. O., and Akagi, S. K.: Pitfalls with the use of enhancement ratios or normalized excess mixing ratios measured in plumes to characterize pollution sources and aging, *Atmos. Meas. Tech.*, 6, 2155–2158, 110 <https://doi.org/10.5194/amt-6-2155-2013>, 2013.

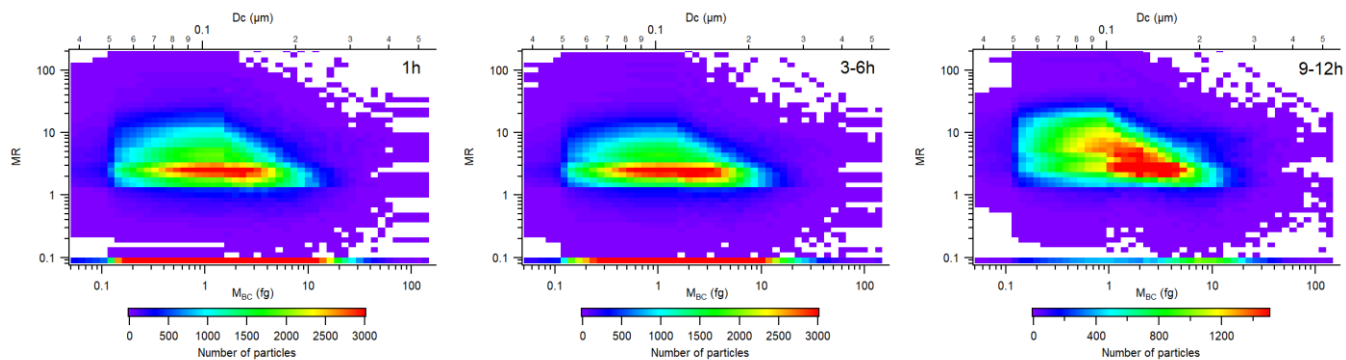


255 **Figure S1:** The vertical distributions of measured horizontal winds, in terms of u (left) and v (right) respectively. The box-and-whisker plots represent the 10th percentile, 25th percentile, median, 75th percentile and 90th percentile in every 200m bin. The dots are the mean values in every 200m bin.

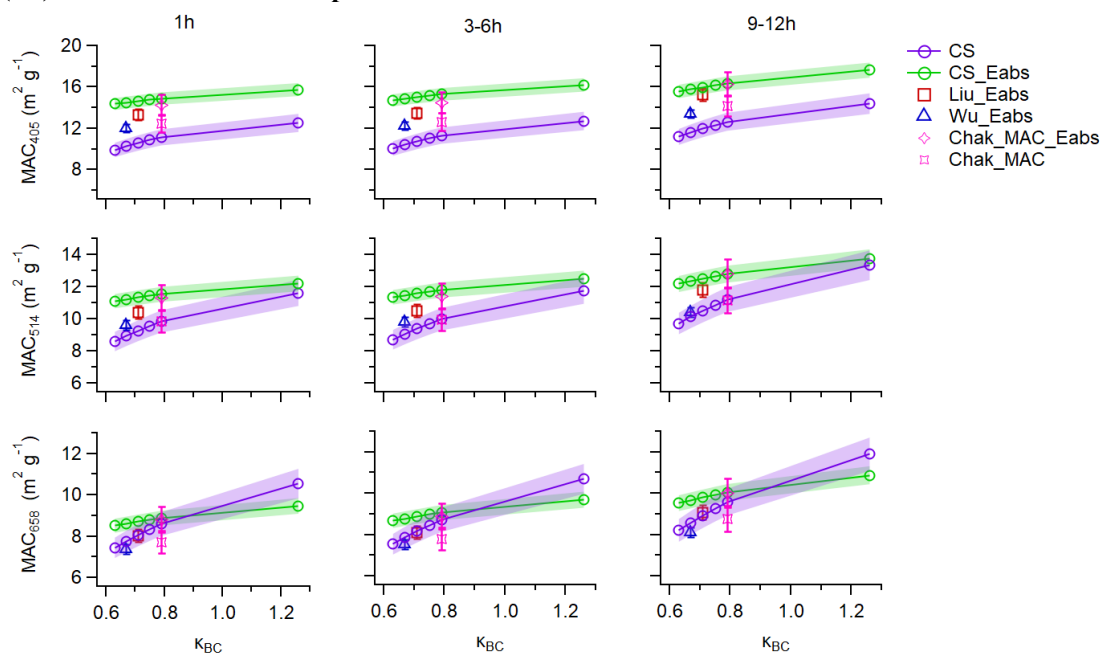


260 **Figure S2:** Time series of measured mass concentrations of non-refractory aerosol species from the AMS and BC from the SP2, and also measured CO and CO₂ mixing ratios, in each flight (Fig. S2a for C005, Fig. S2b for C006 and Fig. S2c for C007). The shaded area are selected smoke plumes at different ages. AMS data for flight C006 is not available as the vacuum pump overheated during this flight. CO was measured using an AeroLaser AL5002 Vacuum-

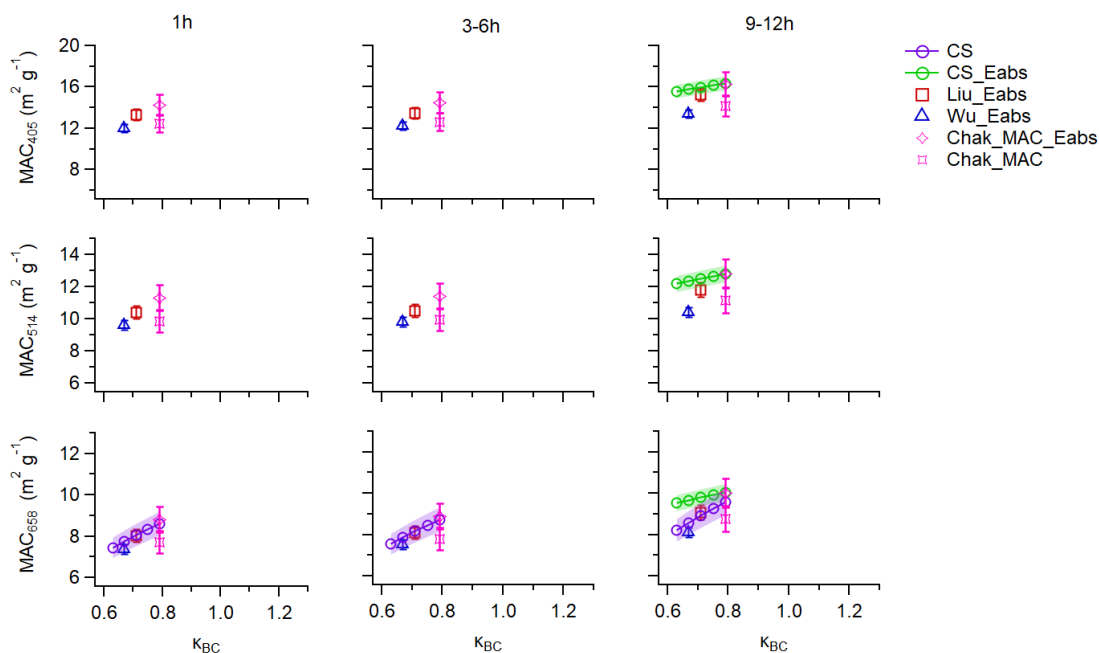
UV fast fluorescence instrument, CO₂ was measured using a Fast Greenhouse Gas Analyser (FGGA).



265 **Figure S3: 2-D distribution of BC mass (M_{BC} , bottom axes) and mixing state (MR, left axes) in sampled smoke plumes with different ages, corrected for the size-dependent detection efficiency of the instrument. Equivalent values of core diameter (D_c) are also shown on the top axis.**



270 **Figure S4: The simulated MAC at 405 (top panels), 514 (middle panels) and 658 (bottom panels) nm wavelengths, assuming the BC mass and mixing states measured in selected smoke plumes at different ages. These MACs were simulated using different optical schemes, assuming non-absorbing coatings. The green and purple markers and lines represent the simulated MACs from ‘CS’ and ‘CS-EAbs’, as a function of the imaginary component of the BC refractive index (k_{BC}). The blue, red and pink markers represent the simulated MACs from different parameterisations. The shades and error bars are simulation uncertainties from the Monte Carlo analysis as Taylor et al. (2020).**



275

Figure S5: The reasonable modelled MAC values for clear-coated BC in selected smoke with different ages, which is selected from the Fig. S4. The upper, middle and bottom panels represent MAC at 405, 514 and 658 nm wavelengths respectively. The green and purple markers and lines represent the simulated MACs from “CS” and “CS-E_{Abs}”, as a function of the imaginary component of the BC refractive index (k_{BC}). The blue, red and pink markers represent the simulated MACs from different parameterisations. The shades and error bars are simulation uncertainties from the Monte Carlo analysis as Taylor et al. (2020).

280

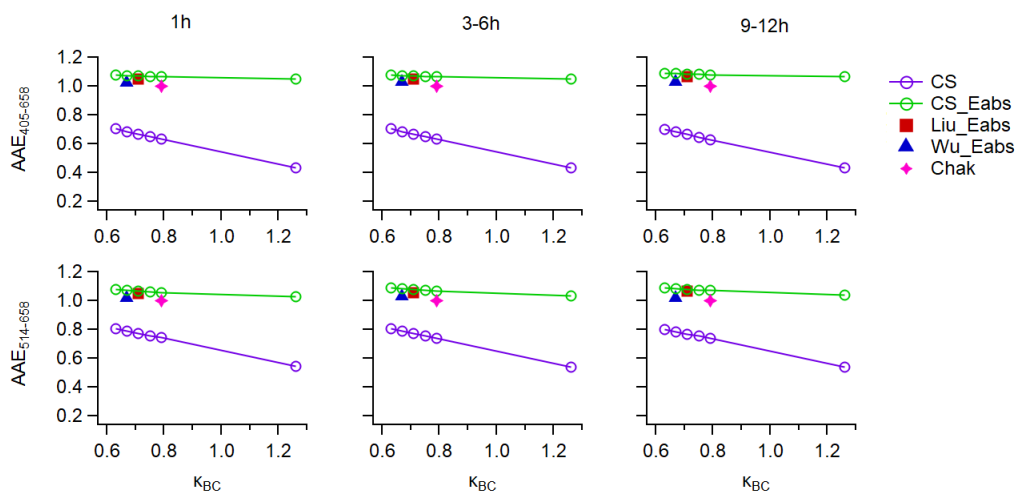


Figure S6: The simulated $AAE_{405-658}$ (top panels) and $AAE_{514-658}$ (bottom panels) values, assuming the BC mass and mixing states measured in selected smoke plumes at different ages. These AAEs were simulated using different optical schemes, assuming non-absorbing coatings. The green and purple markers and lines represent the simulated AAEs from “CS” and “CS-E_{Abs}”, as a function of the imaginary component of the BC refractive index (k_{BC}). The blue, red and pink markers represent the simulated AAEs from different parameterisations.

285

Table S2. The background properties of aerosol sampled out of the plume

Out-of-plume (nearby background)	Over continent (C005)	Over Atlantic (C006)	Over Atlantic (C007)
CO mixing ratio (ppbv)	132 ± 3	132 ± 3	133 ± 2
BC mass ($\mu\text{g m}^{-3}$)	0.38 ± 0.08	0.38 ± 0.08	0.36 ± 0.04
OA mass ($\mu\text{g m}^{-3}$)	1.8 ± 0.5	-	1.6 ± 0.3
nitrate mass ($\mu\text{g m}^{-3}$)	0.18 ± 0.1	-	0.15 ± 0.06
sulfate mass ($\mu\text{g m}^{-3}$)	0.47 ± 0.04	-	0.45 ± 0.1
ammonium mass ($\mu\text{g m}^{-3}$)	0.28 ± 0.1	-	0.26 ± 0.1
chlorine mass ($\mu\text{g m}^{-3}$)	0.07 ± 0.05	-	0.04 ± 0.02
O:C ratio	0.68 ± 0.08	-	0.85 ± 0.08
OM/OC	2.0 ± 0.1	-	2.2 ± 0.1
f_{43}	0.06 ± 0.01	-	0.06 ± 0.01
f_{44}	0.16 ± 0.02	-	0.20 ± 0.02
f_{60}	0.003 ± 0.002	-	0.004 ± 0.002
BC CMD (nm)	106 ± 5	115 ± 6	107 ± 4
BC MMD (nm)	197 ± 23	202 ± 21	191 ± 17
Shell/core ratio	1.4 ± 0.1	1.6 ± 0.1	1.7 ± 0.1
Absolute coating thickness (nm)	30 ± 5	43 ± 7	49 ± 6
Log-normal fitted bulk aerosol CMD (nm)	113	100	124
$B_{\text{Abs-405}}$ (Mm^{-1})	10 ± 1	15 ± 2	12 ± 2
$B_{\text{Abs-514}}$ (Mm^{-1})	6 ± 1	8 ± 1	7 ± 1
$B_{\text{Abs-658}}$ (Mm^{-1})	4 ± 1	5 ± 1	5 ± 1
$\text{AAE}_{405-658}$	2.2 ± 0.4	2.2 ± 0.4	2.1 ± 0.4
$\text{AAE}_{514-658}$	1.9 ± 1	1.8 ± 1	1.8 ± 0.6

Note: OA information was lost in the transported smoke at an age of ~ 3–6 h, as there was no AMS data for the period.